ELSEVIER

Journal of Magnetism and Magnetic Materials 192 (1999) 297–304

Journal of magnetism and magnetic materials

Study of antiferromagnetic NiO using grazing incidence reflectivity and soft X-ray absorption☆

Gerrit van der Laan*

Magnetic Spectroscopy, Daresbury Laboratory, Warrington WA4 4AD, UK

Received 27 March 1998; received in revised form 7 October 1998

Abstract

High-resolution grazing incidence X-ray absorption and reflection spectra near the critical angle for total reflection provide a useful means to refine the analysis of multiplet and charge-transfer satellite structure at the absorption edges for core level excitation. An optical oscillator model can adequately explain the strong spectral changes observed in the region of the Ni 2p edge of NiO epitaxially grown on Mg(1 0 0). The results confirm that NiO is a charge-transfer-type insulator with parameters that relate to the effective superexchange interaction.

PACS: 78.70.Dm; 75.50.Ee; 71.70. − d

Keywords: Antiferromagnets; X-ray spectroscopy; Superexchange; Reflectivity; Electron yield

1. Introduction

The electronic structure of the late 3d transition metal monoxides has been a controversial subject ever since the discovery that these oxides are insulators [1], which is in sharp contrast with one-electron band structure theory [2,3] that predicts them to be metallic. The insulating behaviour is thought to be caused by strong electron correlation effects, resulting in a breakdown of the one-electron picture. According to the Mott–Hubbard model [4,5,47] the large on-site d–d Coulomb repulsion suppresses high-energy charge fluctuations, $d^n + d^n \rightarrow d^{n-1} + d^{n+1}$, which describe the hopping of a d electron between two metal sites. It is important to note that this excitation involves an effective parameter U for the repulsion energy, which is strongly reduced from its atomic value due to the influence of screening and covalence in the solid. For example, U is 6.7 eV in bulk NiO, while the atomic value would be 18 eV. Although the Mott–Hubbard model explains correctly the existence of a wide optical gap, it fails to give a quantitative account of the optical gap [6] and X-ray spectra [7] of 3d transition metal oxides, halides and chalcogenides. The optical gap in these materials is determined by the charge-transfer energy, Δ, which is the energy cost to transfer an electron from

* Tel.: + 0-1925-603-448; fax: + 0-1925-603-124; e-mail: g.vanderlaan@dl.ac.uk.

☆Invited Paper presented at the "International Workshop on Soft X-ray Magneto-Optics", Institut für Angewandte Physik, Heinrich-Heine-Universität Düsseldorf, 13 November 1997.

0304-8853/99/$ – see front matter
PII: S0304-8853(98)00541-1

a ligand to a metal ion, i.e. $d^n \rightarrow d^{n+1}\underline{L}$, where $\underline{L}$ denotes a hole in the ligand band [8]. Although NiO was originally believed to be a Mott–Hubbard insulator, i.e. with a gap determined by U, Fujimori et al. [9] showed by a cluster model calculation for the valence band photoemission that this material is actually a charge-transfer insulator. The combination of photoemission and inverse photoemission gives an experimental value for the band gap of 4.3 eV, [10,11] while density functional theory predicts only a gap of 0.3 eV [12]. The electron transport properties are rather well described by impurity model calculations as a function of the ligand p-band width, w, and the p–d hybridisation with hopping matrix element, t. The virtual charge excitations which couple the spins on the different metal ions can be described by an Anderson superexchange model [13]. In terms of the ground state parameters t, Δ, and U, the effective superexchange interaction J can be written as [14]

$$J \approx -\left(\frac{2t^2}{\Delta}\right)^2\left(\frac{1}{U}+\frac{1}{\Delta}\right), \tag{1}$$

where for simplicity multiplet effects have been neglected. Neutron scattering gives a value of $J =$ 19 meV for NiO, [15,16] which agrees very well with the values of $U = 6.7$ eV, $\Delta = 6.2$ eV and $t = 0.5$ eV obtained from the analysis of X-ray core level spectroscopies with impurity model calculations[1] [17,18].

Thin film structures containing transition metal oxides have sought-after magnetic properties, such as exchange biasing [19]. Considerable experimental effort has been put into this phenomenon because of its technological significance in domain stabilisation of magnetoresistive devices, such as spin valves [20]. The bulk magnetic structure of NiO below the Néel temperature of 520 K consists of ferromagnetically (FM) aligned spins in the (1 1 1) planes, which are antiferromagnetically (AFM) stacked with respect to each other. There are 24 different magnetic domains in total. Four principle, so-called T, domains can be distinguished corresponding to the four possible [1,1,1] directions which can be further divided into three S domains corresponding to the three possible $[1,1,\bar{2}]$ directions with two different spin directions. The exchange biasing is attributed to the interfacial exchange interaction between FM and AFM spins of the antiferromagnetic domains. AFM materials in contact with FM materials can give rise to hysteresis loop shifts away from the zero-field axis. Originally, it was thought that the AFM spins order in a single domain with all interfacial AFM spins perfectly aligned in a single direction parallel to the FM spins, resulting in a net moment due to the uncompensated AFM spins at the interface. However, measurements show that biasing fields are typically two orders of magnitude smaller than expected. Recent theoretical work, supported by neutron diffraction, suggests domain formation resulting from a 90° coupling between the AFM and FM moments [21].

Core level spectroscopy studies using synchrotron radiation can provide important element-specific information about the electronic and magnetic ground state of composite materials. Magnetic X-ray dichroism (MXD) and X-ray resonant magnetic scattering have found wide application in the study of magnetic properties of ferro-, ferri- and antiferromagnetic systems [22–25,48]. Sum rules allow the separation of the total magnetic moment into an orbital and spin contribution [26–28]. However, in X-ray absorption the true line shape can be strongly distorted depending on the specific detection technique [29–31]. Saturation effects occur near the absorption edge if the mean escape depth of the detected particles, such as electrons in the case of total electron yield or photons in the case of fluorescence detection, cannot be neglected with respect to the X-ray attenuation length [32]. For strong absorption structures, such as the $3d \rightarrow 4f$ in rare earths, these effects can even show up at normal incidence [29]. Sometimes, additional information can be obtained about the underlying decay mechanism that causes the strong absorption. By analysing the total electron yield as a function of incidence angle, van der Laan and Thole [30] obtained the La 3d autoionisation lifetime width and Vogel et al. [33,49] assessed the mean electron escape depth.

[1] The parameters U and Δ in this paper are defined with respect to the lowest level of the configuration, whilst in Refs. [17,18] they are defined to the average, $E_{av} = E(^3F) + 1.3$ eV. Furthermore, the six neighbours in NiO result in an effective transfer integral of $T = t\sqrt{6}$.

In this paper, we will compare grazing incidence reflectivity and total electron yield measurements using linearly polarised light. In Refs. [34,35] it was shown that the strong spectral distortions at grazing incidence make it possible to reveal the weaker structures in the absorption spectrum. In the case of NiO this provides an important verification for the charge transfer model. The Ni 2p absorption structure is ideally suited since it displays an atomic-like multiplet structure which is dominated by a small number of intense peaks, while weaker structures are unresolved. These weaker structures contain important information concerning the details of the ground state electronic structure. A study of the absorption and reflection near grazing incidence makes it possible to observe these hidden transitions. A straightforward optical analysis is sufficient to extract the information concerning the peaks positions and oscillator strengths.

The outline of this paper is as follows. In Section 2 we discuss how the optical constants and oscillator strengths can be extracted from the X-ray absorption spectrum measured in total electron yield and reflection. The origin of the peak structure in the Ni 2p absorption spectrum is described in Section 3. Experimental details about the measurements are given in Section 4. Results of the total electron yield and reflectivity measurements are presented in Section 5. Conclusions are drawn in Section 6.

2. Optical constants

First we discuss how we can extract the optical constants from the absorption spectra.

2.1. Attenuation coefficient

The electric field of the X-rays propagating in a medium can be written as

$$\boldsymbol{E}(\boldsymbol{r},t) = \boldsymbol{E}_0 \mathrm{e}^{\mathrm{i}(\boldsymbol{K}\cdot\boldsymbol{r}-\omega t)} = E_0 \mathrm{e}^{-n''\boldsymbol{K}_0\cdot\boldsymbol{r}} \mathrm{e}^{\mathrm{i}(n'\boldsymbol{K}_0\cdot\boldsymbol{r}-\omega t)} \quad (2)$$

with wave vector $\boldsymbol{K} = \omega n/c = 2\pi n/\lambda_0 = \boldsymbol{K}_0 n$, angular velocity ω, frequency ν, wavelength λ, and velocity c. $\boldsymbol{K}_0$ is the wave vector in vacuum. The complex refractive index of the medium is $n = \sqrt{\varepsilon\mu}$, where the permittivity tensor $\varepsilon = \boldsymbol{D}/\boldsymbol{E}$ and permeability tensor $\mu = \boldsymbol{B}/\boldsymbol{H}$ connect the electric field $\boldsymbol{E}$ and magnetic field $\boldsymbol{B}$ to the electric displacement vector $\boldsymbol{D}$ and magnetic induction $\boldsymbol{H}$, respectively. The complex refractive index can be written as $n = n' + \mathrm{i}n''$ with $(n',n'') \in \{\Re\}$, where the spectral refractive index, n', and extinction coefficient, n'', are connected by a Kramers–Kronig (KK) transformation.

Eq. (2) shows that the intensity is exponentially damped with an attenuation factor

$$\boldsymbol{E}^2(z)/\boldsymbol{E}^2(0) = \mathrm{e}^{-2n''K_0 z} \equiv \mathrm{e}^{-\mu z}, \quad (3)$$

where z is the length in the medium and

$$\mu = 2K_0 n'' = \frac{\pi}{\lambda} n'' = \frac{2\omega}{c} n'' \quad (4)$$

is the absorption or attenuation coefficient.

In principal, n'' can be determined from the decrease in X-ray intensity as a function of sample penetration z. Therefore, measurement of the attenuation of the beam through the sample appears to be the most obvious way to determine the absorption coefficient. Although measurements in transmission mode are indeed standard in the hard X-ray region, they are strenuous to perform in the soft X-ray region. In order to avoid saturation effects caused by the small absorption length, the samples need to be very thin (<100 Å). The preparation of extremely thin samples without pinholes suitable for transmission mode measurements is a difficult task. Therefore, alternative methods based on monitoring the flux of decay products, such as electrons, photons or ions, upon core hole de-excitation are more conceivable. In this case the signal is not necessarily proportional to the absorption cross section.

2.2. Electron yield detection

The probability that an electron excited at depth z will reach the detector is given by $C\mathrm{e}^{-z/d}$, where the factor C takes into account the detector efficiency. The mean electron escape depth d is independent of z but depends weakly on the kinetic energy of the electron.

The quantum yield as a function of depth can be written as

$$Y(z) = C\mu_\theta e^{-z\mu_\theta} e^{-z/d}, \tag{5}$$

where $\mu_\theta = \mu/\sin\theta$ is the effective absorption depth at a grazing angle θ of the incident X-rays with respect to the surface. For a film of thickness t the quantum yield per incident photon is given by

$$\begin{aligned} Y &= C(1-R)\int_0^t Y(z)\mathrm{d}z \\ &= C(1-R)\frac{\mu_\theta d}{1+\mu_\theta d}\left[1 - e^{-(1+\mu_\theta d)t/d}\right] \end{aligned} \tag{6}$$

where also the correction for reflection of the X-rays at the sample surface is taken into account. For s-polarised light the reflectivity is given by the Fresnel equation [36]

$$R = \left|\frac{\cos\theta - \sqrt{n^2 - \sin^2\theta}}{\cos\theta + \sqrt{n^2 - \sin^2\theta}}\right|^2. \tag{7}$$

2.3. Classical oscillator model

A simple way to represent the interaction of the core electrons with the X-rays is provided by using a classical oscillator model. The equation of motion for an oscillator with resonance frequency ω_0 and damping constant $m\Gamma$ is given by Hooke's law as [36]

$$\ddot{\boldsymbol{r}} + \Gamma\dot{\boldsymbol{r}} + \omega_0^2\boldsymbol{r} = -\frac{e}{m}\boldsymbol{E}_0 e^{i\omega t}, \tag{8}$$

which gives the solution

$$(\omega_0^2 - \omega^2 + i\Gamma\omega)\boldsymbol{r} = -\frac{e}{m}E(t). \tag{9}$$

The scalar polarisation (dipole moment per unit volume) is $P = -Ner = \alpha\varepsilon_0 E$, so that

$$\begin{aligned} \varepsilon &\equiv 1 + \alpha \\ &= 1 + \frac{Ner}{\varepsilon_0 E} \\ &= 1 + \frac{Ne^2}{m\varepsilon_0}\frac{1}{\omega_0^2 - \omega^2 + i\Gamma\omega}. \end{aligned} \tag{10}$$

The transition from classical oscillators to atoms is accomplished by replacing N by $N_i f_{ij}$ and ω_0 by ω_{ij}, where N_i is the density of atoms in the ground state with oscillator strength f_{ij}. The latter is a dimensionless quantity which represents the effective number of electrons per atom for a transition at frequency ω_{ij}. In the spectral region near the absorption edge we can make the approximations $\omega_{ij}^2 - \omega^2 \to 2\omega_{ij}(\omega_{ij} - \omega)$ and $\omega\Gamma \to \omega_{ij}\Gamma$, so that

$$n' \propto 1 + \frac{N_i e^2}{m\varepsilon_0}\sum_j \frac{f_{ij}(\omega_{ij} - \omega)}{(\omega_{ij} - \omega)^2 + \Gamma_{ij}^2}, \tag{11}$$

$$n'' \propto \frac{N_i e^2}{m\varepsilon_0}\sum_j \frac{f_{ij}\Gamma_{ij}}{(\omega_{ij} - \omega)^2 + \Gamma_{ij}^2}. \tag{12}$$

Thus the spectral distribution of n' is a sum over lines with a dispersive shape, whereas that of n'' is given by a sum over Lorentzians with energy positions ω_{ij} and half-widths Γ_{ij}.

The imaginary and real part of the spectral refractive index in Eqs. (11) and (12) which are mutually related by KK transformation, provide directly the spectra in which we are interested. The absorption coefficient is proportional to the imaginary part, cf. Eq. (4). The angular-dependent reflectivity is a function of both imaginary and real part, cf. Eq. (7). Applying these equations avoids the explicit use of KK transformations, which are known to suffer from problems of slow convergence and the necessity of choosing high cutoff values for the energy [37,38].

3. Origin of the peak structure

The 2p absorption spectrum of NiO is shown in Fig. 1. Its structure has been explained in detail in Ref. [17], so that it is only briefly touched here. The L_3 main structure (peak a and b) is due to transitions into $\underline{2p}_{3/2}3d^9$ final states and the L_2 main structure (peak f and g) is due to transitions into $\underline{2p}_{1/2}3d^9$ states. Both edges display a multiplet splitting into roughly two peaks. For a large part this splitting is due to the 2p–3d exchange interaction [38–40]. The weak structures between the two edges (peak c and d) are due to excitations into $\underline{2p}_{3/2}3d^{10}\underline{L}$ final states. The broad structure around 866 eV (peak e) is caused by the onset of the $\underline{2p}_{3/2}3d^9\underline{L}\ k$ final states. Compared with the main L_3 peak, these final states contain an extra ligand hole and a continuum electron. This

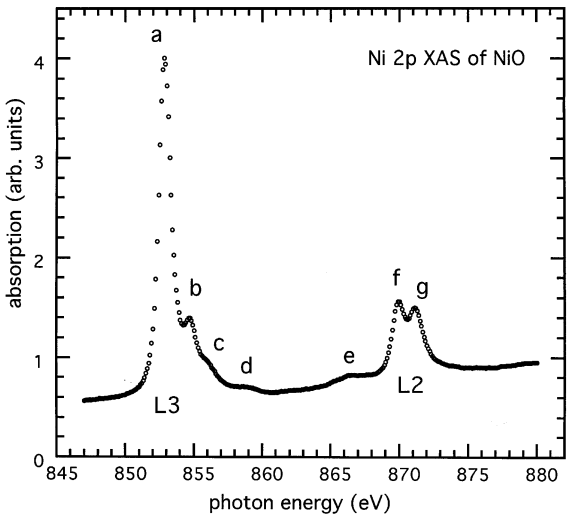

Fig. 1. Ni 2p absorption spectrum of NiO measured in total electron yield with the X-rays at normal incidence. See text for peak assignment.

results in a relative energy at the onset of $\varepsilon_L + Q$, where ε_L is the ionisation energy of a ligand 2p electron (~ 6 eV) and Q is the screened 2p–3d Coulomb interaction (~ 7 eV).

The peak ratio in the L_2 structure is very sensitive to the orientation of the linear polarisation vector of the X-rays with respect to the spin orientation. This makes it interesting to study NiO with magnetic X-ray linear dichroism (MXD) as was demonstrated by Kappert et al. [41] and Alders et al. [42]. A preferred spin orientation can be imposed by thin film epitaxial growth on a MgO(1 0 0) single crystal substrate, which due to the interface anisotropy results in a preferential spin in the $[\pm 2, \pm 1, \pm 1]$ directions. In the isotropic spectrum (cf. Fig. 1) the low-energy peak (f) has the highest intensity. However, for ordered samples on MgO the relative ratio of the two peaks changes strongly with the direction of the linear polarisation and the intensity of the two peaks can be interchanged.

4. Experimental

The high-resolution spectrum shown in Fig. 1 was obtained at the synchrotron radiation source (SRS) at Daresbury Laboratory using beamline 3.4 equipped with a double beryl crystal monochromator [43]. The sample was a cleaved NiO single crystal measured with total electron yield and the X-ray beam at normal incidence.

Total yield and reflectivity measurements at grazing incidence (Fig. 2) were done at the SRS undulator beam line 5U.1, which is equipped with a variable-included-angle plane-grating monochromator [44]. The vertical entrance aperture of the monochromator was restricted to give a high linear polarisation ($>90\%$). Angular measurements were performed using a θ–2θ reflectometer operated under high vacuum conditions. In this apparatus the sample deflects the beam vertically while the rotation axis is horizontal and parallel to the electric vector of the X-rays. The beam reflected from the sample was detected by a slitted GaAsP/Au photodiode. The total electron yield was monitored using a high current channeltron positioned directly above the sample. A grid over the front of the channeltron was biased at $+200$ V to ensure a good collection efficiency. The sample and the photodiode could be independently rotated using high precision rotary tables with 0.001° resolution. The angular position of these tables was controlled via stepping motors under computer control. The photon energy was scanned at different θ and the reflectivity and electron yield was recorded simultaneously. In order to avoid MXD effects, the direction of the electric vector was kept horizontally by using s-polarised light and only the grazing angle θ was changed.

For the experiments on line 5U.1 the sample consisted of 27 monolayers NiO epitaxially grown in a layer-by-layer fashion on a single crystal of MgO(1 0 0) as monitored by reflection high-energy electron diffraction [45]. NiO and MgO exhibit a face-centered-cubic rocksalt (NaCl) structure with lattice constants of 4.176 and 4.212 Å, respectively, resulting in a lattice mismatch of 0.85%.

5. Results

The reflectivity and total electron yield spectra at the Ni 2p absorption edges are shown in Fig. 2 as a function of the angle θ between the (1 0 0) plane

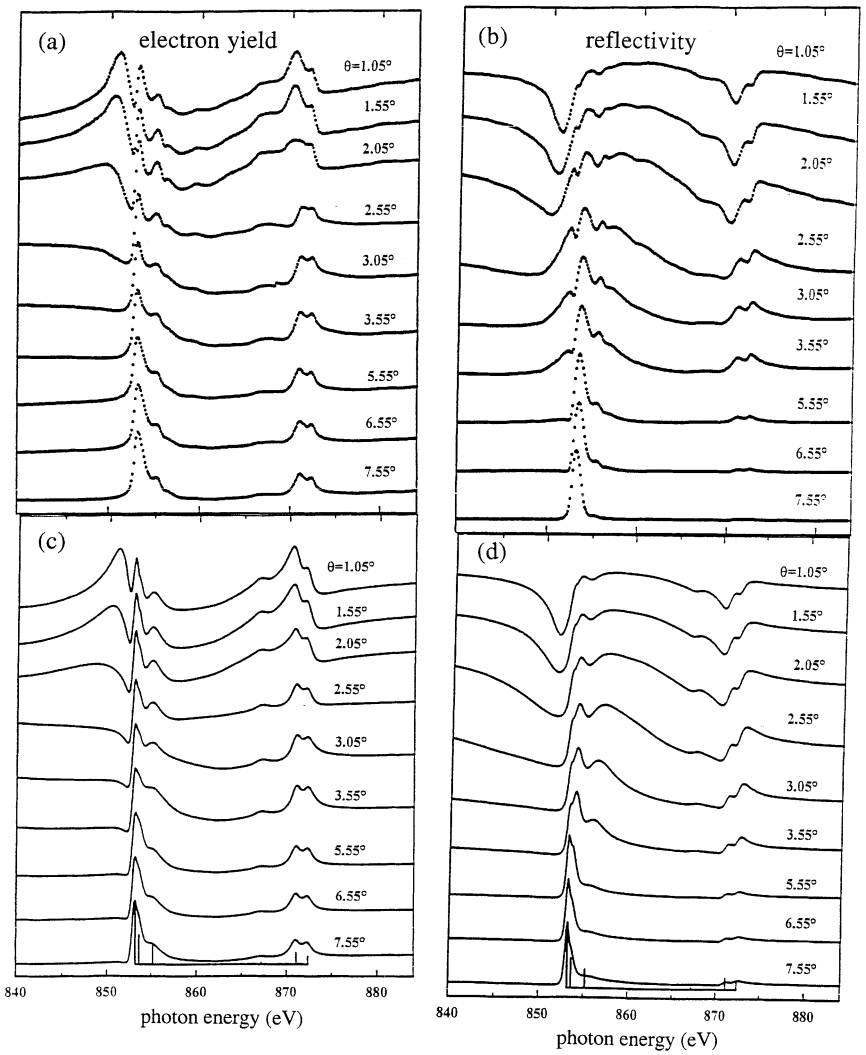

Fig. 2. Glancing angle (θ) dependence at the Ni 2p absorption edge of 27 ML NiO on MgO(1 0 0) single crystal using s-polarised light. (a) measured total electron yield; (b) measured reflectivity; (c) theoretical total electron yield; and (d) theoretical reflectivity using the Lorentzian lines indicated by the sticks under the bottom spectrum. All spectra have been normalised.

and the direction of the incident s-polarised X-rays. The top panels show the experimental results and the bottom panels show the simulations computed using the optical model. The observed spectra exhibit a strong distortion compared to the spectrum in Fig. 1, which was measured at normal incidence. In the electron yield spectra (Fig. 2a) the most intense peak is suppressed at grazing angles due to the influence of saturation and all features tend to reach comparable heights. At very low grazing angles a dip evolves in the pre-edge, preceded by a bump with its maximum shifting towards higher photon energy for reduced angles of incidence. This bump reveals the critical angle for total reflection. When the photon energy is scanned towards the L_3 edge, the absorption coefficient increases and at sufficiently small grazing angles the condition for total reflection can be reached. Then, apart from the evanescent wave, no light will penetrate inside the sample. Thus the total electron yield will be

reduced, even though the absorption coefficient is increased for energies closer to the L_3 edge. This effect suppresses the strongest multiplet lines and as a result the weaker ones, which are normally eclipsed, are now distinguishable. This is nicely demonstrated for the charge-transfer satellite structures above the L_3 edge.

Fig. 2b shows the measured reflectivity as a function of the grazing angle. At large glancing angles ($\theta > 6^\circ$) the reflectivity spectrum displays only the most intense feature of the electron yield L_3 spectrum at 852 eV. At smaller angles an extra peak in the pre-edge of the L_3 evolves. It is interesting to note that at low glancing angles ($\theta < 2^\circ$) the reflectivity spectrum resembles the electron yield spectrum but with its shape *upside down*. This is because the sum of absorbed and reflected light is constant with energy.

Only a few oscillators, which are shown at the bottom of Fig. 2c and Fig. 2d, were included in the calculation. This covers globally in Fig. 1 the main structures a and b of the L_3 edge and the structures f and g of the L_2 edge, as well as the feature e. Thus, weak satellite features, such as c and d, were not included. This leads to some prominent differences in the region between the L_3 and L_2 peaks, namely the calculated spectra are smooth while the experimental spectra show quite a lot of weak structure, especially at smaller angles. It clearly demonstrates that low-intensity features become more distinct at smaller angles. The origin of the features between the L_3 and L_2 peaks can be traced to the $\underline{2p}_{3/2}3d^{10}\underline{L}$ final states, which have higher photon energies than the $\underline{2p}_{3/2}3d^9$ final states due to the core-valence Coulomb interaction. Also the shapes of experimental and calculated reflectivity spectra in the 2.5–3.5° near the onset of the main line are somewhat different. It is possible that the use of a band form instead of discrete oscillators in the model might give an improvement.

In order to predict the angle dependence over the spectral region of interest background and line shape broadening effects should be taken into account. In the most simple case the lifetime broadening can be simulated by a Lorentzian line shape, while the instrumental broadening can be represented by a Gaussian line shape. Other mechanisms, such as autoionisation, can result in a Fano line shape which requires also an asymmetry parameter [46]. Fig. 2c shows a comparison of the best theoretical fit using Eq. (6) to the angular-dependent electron yield data, where the escape depth of the electrons was somewhat arbitrarily set to 50 Å [35]. The overall agreement with experiment, as shown in Fig. 2, is very good. Simulations using a Fano line shape did not significantly improve the fitting, suggesting that the coupling of the final state multiplet with the continuum states is small. Fig. 2d shows the theoretical reflectivity spectra as obtained from fitting of the electron yield spectra, where again a good agreement is reached.

6. Conclusions

Grazing incidence absorption and reflection measurements in the soft X-ray region display dramatic changes the spectral line shape which can be explained using a simple optical model based on Fresnel's equation. The results provide detailed information about the underlying multiplet structure at the X-ray absorption edges. The critical angle behaviour of the multiplet structure has been exploited to study low-intensity satellite structures. The method provides a novel way to study the magnetic ground state of transition metal compounds.

Acknowledgements

I would like to acknowledge the collaboration with K.C. Cheung, G.E. van Dorssen, M.D. Roper, H.A. Padmore, J. Vogel, M. Sacchi, D. Alders, S.D. Peacor, T. Hibma, B.T. Thole, and G.A. Sawatzky.

References

[1] H.J. de Boer, E.J.W. Verwey, Proc. Phys. Soc. London A 49 (1937) 59.
[2] F. Bloch, Z. Phys. 57 (1929) 545.
[3] A.H. Wilson, Proc. Phys. Soc. London A 133 (1931) 458.
[4] N.F. Mott, Proc. Phys. Soc. London A 62 (1949) 416.
[5] J. Hubbard, Proc. Phys. Soc. London A 277 (1964) 237.
[6] J. Zaanen, G.A. Sawatzky, J.W. Allen, Phys. Rev. Lett. 55 (1985) 418.

[7] G. van der Laan, R.A.D. Pattrick, C.M.B. Henderson, D.J. Vaughan, J. Phys. Chem. Solids 53 (1992) 1185.
[8] G. van der Laan, C. Westra, C. Haas, G.A. Sawatzky, Phys. Rev. B 23 (1981) 4369.
[9] A. Fujimori, F. Minami, Phys. Rev. B 30 (1984) 957.
[10] G.A. Sawatzky, J.W. Allen, Phys. Rev. Lett. 53 (1984) 2339.
[11] J.M. McKay, V.E. Henrich, Phys. Rev. Lett. 53 (1984) 2343.
[12] K. Terakura, A.R. Williams, T. Oguchi, J. Kübler, Phys. Rev. Lett. 52 (1984) 1830.
[13] P.W. Anderson, Phys. Rev. 115 (1959) 2.
[14] W. Geertsma, Ph.D Thesis, University of Groningen, The Netherlands (1986).
[15] M.T. Hutching, E.J. Samuelsen, Phys. Rev. B 6 (1972) 3447.
[16] R.E. Dietz, G.I. Parisot, A.E. Meixner, Phys. Rev. B 4 (1971) 2302.
[17] G. van der Laan, J. Zaanen, G.A. Sawatzky, R.C. Karnatak, J.M. Esteva, Phys. Rev. B 33 (1986) 4253.
[18] J. Zaanen, C. Westra, G.A. Sawatzky, Phys. Rev. B 33 (1986) 8060.
[19] R. Jungblut, R. Coehoorn, M.T. Johnson, J. aan de Stegge, A. Reinders, J. Appl. Phys. 75 (1994) 6659.
[20] B. Dieny, V.S. Speriosu, S.S.P. Parkin, B.A. Gurney, D.R. Wilhout, D. Mauri, Phys. Rev. B 43 (1991) 1297.
[21] Y. Ijiri, J.A. Borchers, R.W. Erwin, S.H. Lee, P.J. van der Zaag, R.M. Wolf, Phys. Rev. Lett. 80 (1998) 608.
[22] B.T. Thole, G. van der Laan, G.A. Sawatzky, Phys. Rev. Lett. 55 (1985) 2086.
[23] G. van der Laan, B.T. Thole, G.A. Sawatzky, J.B. Goedkoop, J.C. Fuggle, J.M. Esteva, R.C. Karnatak, J.P. Remeika, H.A. Dabkowska, Phys. Rev. B 34 (1986) 6529.
[24] J.P. Hannon, G.T. Trammell, M. Blume, D. Gibbs, Phys. Rev. Lett. 61 (1988) 1245.
[25] C.C. Kao, C.T. Chen, E.D. Johnson, J.B. Hastings, H.J. Lin, G.H. Ho, G. Meigs, J.M. Brot, S.L. Hulbert, Y.U. Idzerda, C. Vettier, Phys. Rev. B 50 (1994) 9599.
[26] B.T. Thole, P. Carra, F. Sette, G. van der Laan, Phys. Rev. Lett. 68 (1992) 1943.
[27] P. Carra, B.T. Thole, M. Altarelli, X. Wang, Phys. Rev. Lett. 70 (1993) 694.
[28] G. van der Laan, Phys. Rev. B 57 (1998) 112.
[29] B.T. Thole, G. van der Laan, J.C. Fuggle, G.A. Sawatzky, R.C. Karnatak, J.M. Esteva, Phys. Rev. B 32 (1985) 5107.
[30] G. van der Laan, B.T. Thole, J. Electron Spectrosc. Relat. Phenomen. 46 (1988) 123.
[31] V. Chakarian, Y.U. Idzerda, C.T. Chen, Phys. Rev. B 57 (1998) 5312.
[32] W. Gudat, C. Kunz, Phys. Rev. Lett. 29 (1972) 169.
[33] J. Vogel, M. Sacchi, Phys. Rev. B 49 (1994) 3230.
[34] J.M. André, A. Marquet, R. Barchewitz, Phys. Rev. B 25 (1982) 5671.
[35] D. Alders, T. Hibma, G.A. Sawatzky, K.C. Cheung, G.E. van Dorssen, H.A. Padmore, M.D. Roper, G. van der Laan, J. Vogel, M. Sacchi, J. Appl. Phys. 82 (1997) 3120.
[36] M. Born, E. Wolf, Principles of Optics, Pergamon press, New York, 1975.
[37] N. Mainkar, D.A. Browne, J. Callaway, Phys. Rev. B 53 (1996) 3692.
[38] M. Sacchi, C.F. Hague, L. Pasquali, A. Mirone, J.-M. Mariot, P. Isberg, E. Gullikson, J.H. Underwood, Phys. Rev. Lett. 81 (1998) 1521.
[39] G. van der Laan, B.T. Thole, G.A. Sawatzky, M. Verdaguer, Phys. Rev. B 37 (1988) 6587.
[40] G. van der Laan, C.M.B. Henderson, R.A.D. Pattrick, S.S. Dhesi, P.F. Schofield, E. Dudzik, D.J. Vaughan, unpublished.
[41] R.J.H. Kappert, J. Vogel, M. Sacchi, J.C. Fuggle, Phys. Rev. B 48 (1993) 2711.
[42] D. Alders, J. Vogel, C. Levelut, S.D. Peacor, T. Hibma, M. Sacchi, L.H. Tjeng, C.T. Chen, G. van der Laan, B.T. Thole, G.A. Sawatzky, Europhys. Lett. 32 (1995) 259.
[43] A.A. MacDowell, J.B. West, G.N. Greaves, G. van der Laan, Rev. Sci. Instr. 59 (1988) 843.
[44] C.S. Mythen, G. van der Laan, H.A. Padmore, Rev. Sci. Instr. 63 (1992) 1313.
[45] S.D. Peacor, T. Hibma, Surf. Sci. 301 (1994) 11.
[46] U. Fano, Phys. Rev. 124 (1961) 1866.
[47] J. Hubbard, Proc. Phys. Soc. London A 281 (1964) 401.
[48] J.P. Hannon, G.T. Trammell, M. Blume, D. Gibbs, Phys. Rev. Lett. 62 (1989) 2644.
[49] J. Vogel, M. Sacchi, J. Electron Spectrosc. Relat. Phenomen 67 (1994) 181.